Available online at www.sciencedirect.com
SCIENCE DIRECT
Biomaterials 27 (2006) 5127–5133
Biomaterials
www.elsevier.com/locate/biomaterials

Interfacial behaviour of strontium-containing hydroxyapatite cement with cancellous and cortical bone

G.X. Ni[a], W.W. Lu[a,*], B. Xu[b], K.Y. Chiu[a], C. Yang[b], Z.Y. Li[a], W.M. Lam[a], K.D.K. Luk[a]

[a]Department of Orthopaedics and Traumatology, The University of Hong Kong, Hong Kong, China
[b]Department of Chemistry, Hong Kong University of Science and Technology, Hong Kong, China

Received 3 January 2006; accepted 18 May 2006
Available online 15 June 2006

Abstract

The bone-bonding behaviors of various biomaterials have been extensively investigated. However, the precise mechanisms of bone bonding have not yet been clarified, and the differences in interfacial behaviors of biomaterial bonding with cancellous bone and cortical bone have not yet been understood. In this study, strontium-containing hydroxyapatite (Sr-HA) cement, in which 10% calcium ions were substituted by strontium, was performed in a rabbit hip replacement model. Six months later, the morphology and chemical composition of interfaces between Sr-HA cement with cancellous bone and cortical bone were evaluated by field emission scanning electron microscopy (FESEM) and time-of-flight secondary ion mass spectrometry (ToF-SIMS). Remarkable differences between these two interfaces were suggested both in morphology and chemical compositions. An apatite layer was found between Sr-HA cement and cancellous bone with a thickness of about 70 μm. However, only a very thin interface (about 1 μm) was formed with cortical bone. As for the cancellous bone/cement interface, high ions intensity of Ca, P, Sr, Na, and O were confirmed by FESEM-EDX and ToF-SIMS. Differences in morphology and chemical component between these two interfaces provided convincing evidences for the proposed dissolution–precipitation coupling mechanism in the formation of biological apatite.

Keywords: Strontium-containing hydroxyapatite bone cement; Bone-bonding behaviors; Interface; Mechanism; Chemical composition

1. Introduction

Bioactive materials are classified into surface-active materials (e.g., bioglass, ceravital, hydroxyapatite (HA), apatite-and wollastonite-containing glass-ceramic (A-W GC)) and resorbable materials (e.g., β-tricalcium phosphate (β-TCP), calcite) [1]. All these materials have been reported to bond to bone tightly [2–7], but the precise mechanisms of bone bonding have not yet been clarified. Many investigators have examined the interface between bioactive materials and bone using scanning electron microscopy (SEM) and transmission electron microscopy (TEM) [8–15]. Surface-active ceramics bonded to bone through an intervening apatite layer, dissolution–precipitation mechanism is commonly proposed for the formation of biological apatite. This intervening layer is speculated to be formed by dissolution of some components of the glassy phase of the materials with precipitation of apatite crystals on their surface. In resorbable ceramics, however, calcified bone reaches the chemically and biologically degraded ceramics surface, eventually making direct ceramic–bone contact resulting in mainly mechanical bonding by interlocking.

As for HA, although classified as a surface-active ceramic, it bonds to bone sometimes directly and sometimes through an intervening apatite layer that is very thin and indistinct. The mechanism of the formation of the intervening apatite layer may be different from that of other surface-active materials because of its low solubility [8]. From TEM observation of HA implants, Orly et al. [16] and Daculsi et al. [17] assumed that epitaxial precipitation of apatite crystals occurred. However, the manner in which HA bonds to bone may vary. The dissolution rate of HA in vivo increased when silicate ions were incorporated into the HA lattice [18]. And the substitution of silicate ions into

*Corresponding author. Tel.: +852 2819 9595; fax: +852 2818 5210.
E-mail address: wwlu@hkusua.hku.hk (W.W. Lu).

0142-9612/$ - see front matter © 2006 Elsevier Ltd. All rights reserved.
doi:10.1016/j.biomaterials.2006.05.030

the HA lattice was further suggested to the morphology of apatite depositions and the timing of their deposition [19]. It was also suggested that the substitution of calcium (Ca) by strontium (Sr) caused a crystal expansion due to the larger atomic radius of Sr—which in turn alters the solubility of the mineral [20,21]. Strontium-containing hydroxyapatite (Sr-HA) cement, a bioactive bone cement developed recently for spinal and bone fracture surgery, consists of Sr-HA powder and bisphenol-α-glycidyl dimethacrylate (Bis-GMA)-based resin, in which 10% calcium ions are substituted by Sr [22,23]. Our previous in vivo study [24] indicated the dissolution of Sr-HA cement and proposed a new dissolution–precipitation mechanism for the formation of the bone-like zone subsequently.

Although the dissolution–precipitation mechanism involved in the formation of biological apatite has been widely advocated, evidence of dissolution of materials is mainly based on results from SEM/TEM observation. Obviously, a compositional image of the intervening layer would provide convincing evidence for this proposed mechanism. Furthermore, the differences in bone-bonding behaviour of bioactive materials are considered to be attributable to the differences in chemical composition, crystallisation and solubility of the materials [8–15]. However, to better understand the mechanism of bone bonding, consideration has to be given to the type of bone to which the materials are required to bond. Cortical bone and cancellous bone differ in vascularity and density as well as mechanical properties [25,26]. This might result in different bone-bonding behaviour of biomaterial to cancellous or cortical bone. In a rabbit hip replacement model, we previously demonstrated that Sr-HA cement bonded to cancellous bone and cortical bone in different ways, and the nano-mechanical properties of the interfaces differed considerably [27,28]. Therefore, the morphology and chemical composition of the interfaces were examined by field emission scanning electron microscopy (FESEM) and time-of-flight secondary ion mass spectrometry (ToF-SIMS) in the present study—in the hope of providing insights into interfacial behaviours of Sr-HA cement with cancellous bone and cortical bone.

2. Materials and methods

2.1. Preparation of the bone cements

Sr-HA cement was synthesised and characterised as previously reported by our research group [22,23]. Briefly, Sr-HA bioactive bone cement contains a filler blend of mainly Sr-HA powder and a resin blend of bisphenol A diglycidylether dimethacrylate (Bis-GMA) and triethylene glycol dimethacrylate (TEGDMA). In Sr-HA powder, 10% calcium ions were substituted by Sr ions.

2.2. Animal tests

A total of 6 New Zealand white rabbits were used. The institution's guide for the care and use of laboratory animals was followed. The rabbits were 12–14 months old and weighed between 4.5 and 5.5 kg. Both the rearing of these rabbits and the experiments were carried out according to guidelines for animal experiments at the University of Hong Kong. The rabbits underwent unilateral cemented hip hemiarthroplasty with Sr-HA cement by the same experienced orthopaedic surgeon.

After anesthesia and standard skin sterilisation, a straight incision of about 6 cm along the lateral greater trochanter was made on the lateral side of the leg, exposing the coccygeofemoral and lateral great muscles. Then a transverse capsulotomy was made at the level of the joint space. The femoral head was exposed and removed. After that, the femoral medullary canal was reamed, cleaned and dried. Then Sr-HA cement was prepared and injected into the canal through a syringe. Next, the custom-made hip prosthesis was inserted, and the joint was reduced afterwards. The animals were allowed free activity in cages from immediately after the surgery until sacrifice at the sixth month post-operation.

2.3. Sample preparation

At the time of sacrifice, the femur containing the femoral component and the cement was cut into two sections of 5-mm width (1 metaphyseal and 1 diaphyseal section), axial normal to the long axis of the femur, using a high speed, water-cooled saw with a fine diamond coating (EXAKT 300 CP Band System, Norderstedt, Germany). The specimens were dehydrated and fixed in alcohol solutions with concentrations of 70%, 80%, 90%, and 100% for 3 days in each solution, and then cleaned in xylene. The undecalcified samples were embedded in methylmethacrylate at 4 °C. The slow polymerisation of methylmethacrylate to polymethylmethacrylate (PMMA) at low temperature allowed PMMA to fill all the pores in the implant and the cavities in the bone. This ensured the structure of the cement/bone interface remained intact during sectioning and polishing.

After hardening, normal to the long axis of the femur, the specimens were cut using a cutting machine (EXAKT 300 CP Band System, Norderstedt, Germany). Two adjacent sections were selected from each specimen for FESEM and ToF-SIMS.

2.4. Leo 1530 field emission scanning electron microscope

Representative sections were ground further with alumina-coated sand paper to remove the surface staining, and then sputter coated with a 100 Å layer of carbon. These sections were analysed using Leo 1530 field emission scanning electron microscope, a high-resolution FESEM, together with an energy dispersive X-ray analysis (EDX system from OXFORD^2), enabling visualisation and analysis of surface features of material as small as 0.3 μm in diameter. This makes SEM/EDX ideal for analysing materials, minerals, contaminant particles and particles collected by filtration.

2.5. ToF-SIMS

ToF-SIMS measurements were performed on a PHI 7200 (Physical Electronics, USA) spectrometer equipped with two ion guns (Cs^+ for high massresolution spectroscopy and $^{69}Ga^+$ for spatially resolved imaging) and a reflection analyser. SIMS mapping was acquired in both positive and negative ion modes using a 25 keV Ga^+ primary source. To obtain high spatial resolution mapping and to control the surface charging, an ion pulse length of 50 ns was used. SIMS images were generated by collecting a mass spectrum at every pixel (400 μm × 400 μm) as the primary ion beam was rastered across the sample surface. Before starting to collect chemical information, the surface was bombarded using a Ga + DC beam (1.5 nA current) for 20 min to eliminate surface contamination during the process of specimen preparation.

3. Results

SEM micrograph revealed a distinct apatite layer between Sr-HA cement and cancellous bone with a thickness of about 70 μm (bar = 100 μm) (Fig. 1(A)). Line-scan EDX showed calcium and phosphorus contents at the interface were higher than either at cancellous bone or Sr-HA cement. The content of Sr at the interface was similar to Sr-HA cement, and higher than that at cancellous bone (Fig. 1(B)). On the contrary, a very thin and indistinct interface was found between Sr-HA cement and cortical bone, with a thickness of about 1 μm (bar = 10 μm). Under low magnification (952×, Fig. 2(A)), the interface appeared to be a gap. However, with higher magnifications (5560×, Fig. 2(B) and 28720×, Fig. 2(D)), a smooth transitional interface was confirmed. Line-scan EDX analysis revealed that the content of calcium (Ca), phosphorus (P), oxygen (O) and Sr at the interface was lower than those at bone and Sr-HA cement, respectively (Fig. 2(C)).

SIMS mapping of ionic groups provided additional information on ion intensity on bone, Sr-HA cement and the interfaces. Figs. 3(a and b) show the images of the integrated positive and negative secondary ions, and spatial distribution of various ions in an area including cortical bone, Sr-HA cement and their interface. Figs. 3(c and d) show the equivalent images of the integrated positive and negative secondary ions and spatial distribution of various ions in an area including cancellous bone, Sr-HA cement and their interface. Remarkable contrast in ions distribution was found between these two interfaces. Figs. 3(a and b) show the intensity of such ions as Ca, Na, P, PO_2, and O was lower in the cortical bone/cement interface than Sr-HA cement. In contrast, Figs. 3(c and d) show the ion intensity of ions such as Ca, P, Na, O, OH and F was considerably higher in the cancellous bone/cement interface than the Sr-HA cement. As for the Sr ion, lower intensity was found in cortical bone/cement interface than the cement, while similar intensity was indicated in cancellous bone/cement interface to the cement. The image of the integrated secondary ions represents the sum of all ions in the mass spectrum. In most cases, it would give some idea of surface topography. Overall, images from both interfaces clearly revealed much higher ion intensity in cancellous bone/cement interface than in cortical bone/cement interface. From SIMS, results of ion intensity of Ca, P, Sr and O were generally consistent with those from EDX analysis, as shown in Figs. 1 and 2.

4. Discussion

A body of research has demonstrated that different types of biomaterials exhibit different bone-bonding behaviours due to differences in chemical composition, crystallisation and solubility of materials used [8–15]. However, little attention has been paid to the *type* of bone to which the material bonds. For the first time, this study demonstrates the difference in morphology and chemical composition of the interfaces of Sr-HA cement bonding to cancellous bone and cortical bone. On one hand, Sr-HA cement bonded to cancellous bone through a distinct intervening apatite layer with a thickness of about 70 μm. Yet quite narrow and indistinct junction (only about 1 μm wide) was found between Sr-HA cement and cortical bone. On the other, however, remarkable contrast was indicated for the chemical composition between two interfaces, with EDX and ToF-SIMS both providing information of chemical composition of interface between the biomaterial and bone.

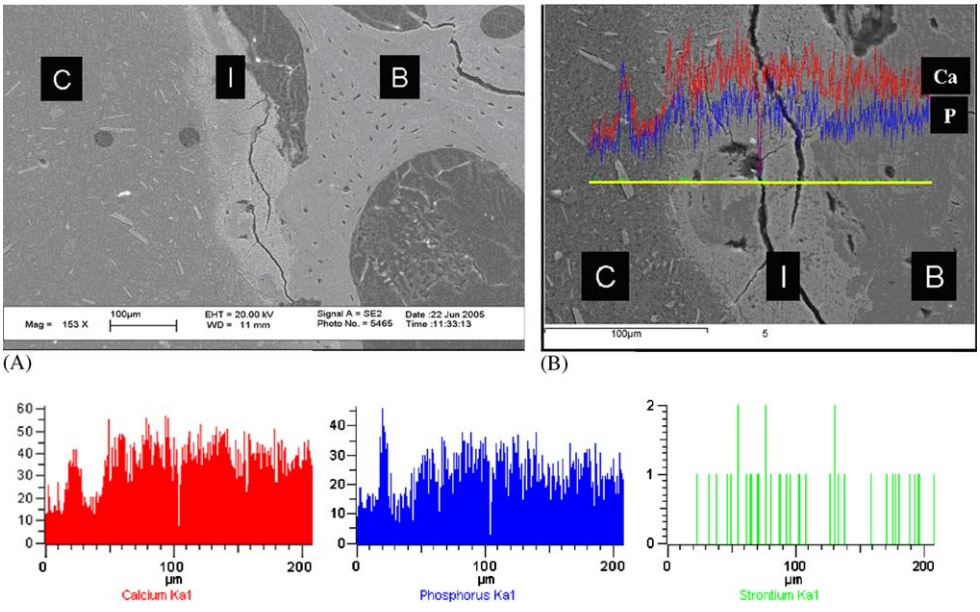

Fig. 1. SEM micrograph and line-scan EDX in an area including cancellous bone, Sr-HA cement, and their interface. B: bone; I: interface; C: Sr-HA cement; Ca: calcium; P: phosphorus.

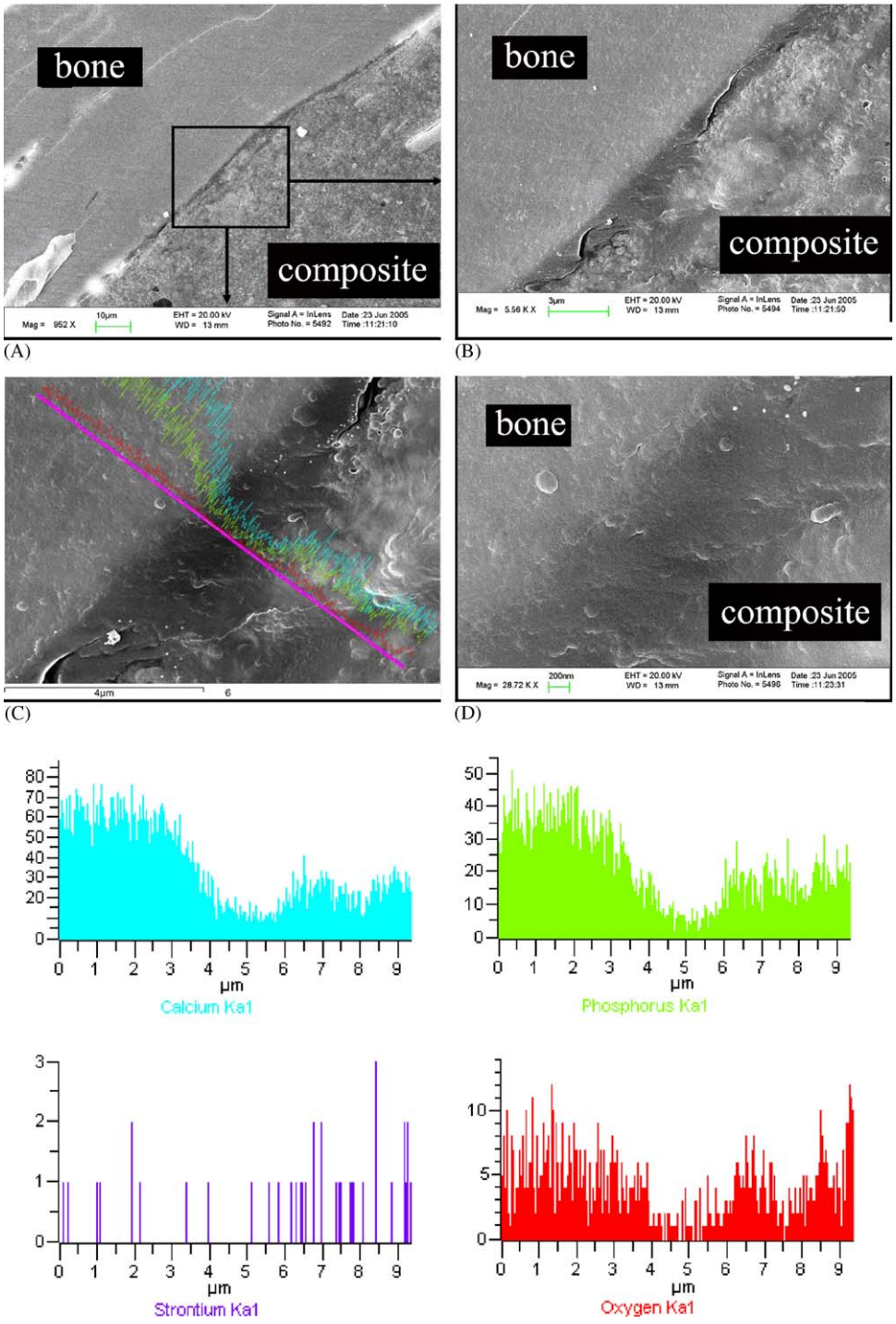

Fig. 2. FESEM microscopy and line-scan EDX in an area of cortical bone, Sr-HA cement, and their interface. B: bone; I: interface; C: Sr-HA cement.

Compared to the cortical bone/Sr-HA cement interface, considerably higher ion intensity of Ca, P, Na, O and PO_2 was found in the cancellous bone/Sr-HA cement interface. The difference in ion intensity between the two interfaces suggested that the dissolution rate of Sr-HA cement differed when bonding to cancellous bone and cortical bone.

Due to its low solubility, the mechanism of the formation of the intervening apatite layer of HA may be different from that of other surface-active materials [8]. HA sometimes bonded to bone directly and sometimes through an intervening apatite layer that was very thin and indistinct [8,12]. However, the solubility of HA may be different with the change of its structure. Porter et al. [18,19] demonstrated that the dissolution rate of HA in vivo would increase with silicate ions incorporated into the HA lattice, and the differing solubility would lead to a difference in morphology of deposits apposed to implants.

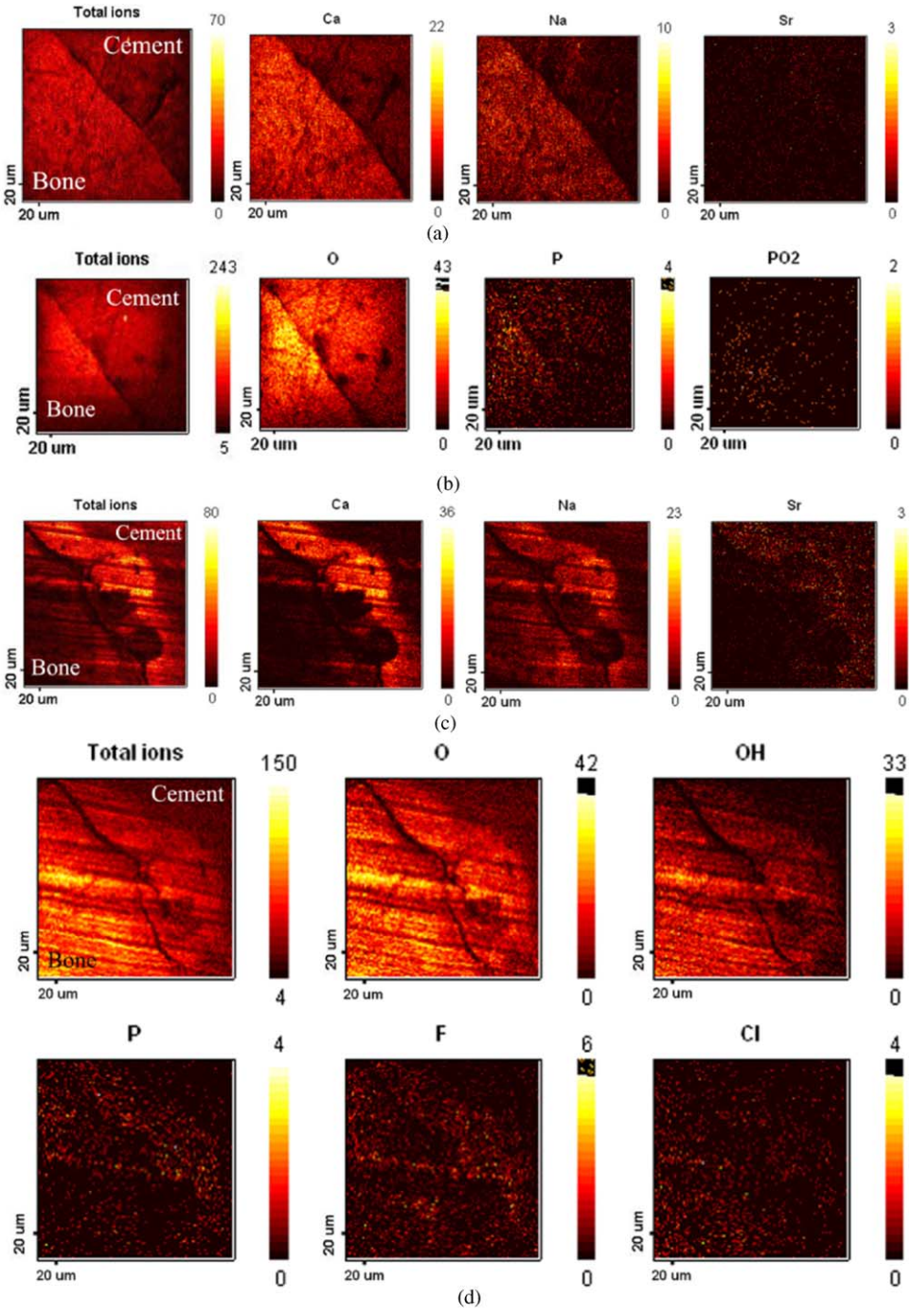

Fig. 3. SIMS images of the integrated positive (a) and negative (b) secondary ions and and spatial distribution of various ions in an area including cortical bone (left side), Sr-HA cement (right side), and their interface; and SIMS images of the integrated positive (c) and negative (d) secondary ions and spatial distribution of various ions in an area including cancellous bone (left side), Sr-HA cement (right side), and their interface (middle).

Also, the substitution of Ca by Sr could cause a crystal lattice expansion due to the larger atomic radius of Sr, which in turn alters the solubility of the mineral [20]. As for the Sr-HA cement used, 10% calcium ions in HA was substituted by Sr. In our previous study [24], Sr-HA cement was injected into rabbit ilium, and dissolution of Sr-HA cement was demonstrated by HRTEM. In the present study, high ion intensity of Ca, P, Na, O, Sr and PO_2 was detected at cancellous bone/Sr-HA cement interface, further indicating a high dissolution rate of Sr-HA bone cement.

Results from this study suggest that a bioactive material's bonding to bone depends not only on the material itself [8–15], but also on the type of bone to which it bonds. Cancellous bone differs from cortical bone in many respects, including vascularity and density [25,26]. Different histological response of Sr-HA cement to cancellous bone and cortical bone was demonstrated in

our previous study [27], in which the osteoclast-like cells were found resorbing the surface of the Sr-HA cement when bonding with cancellous bone, whereas no such phenomenon was observed for cortical bone. This osteoclast-like cells intervening resorbing mechanism as well as the chemical dissolving mechanism may explain why much more ions were released when bonding to cancellous bone than to cortical bone. Differences in chemical compositions between these two interfaces may also account for the differences in morphology of the interfaces. Since the apatite precipitation on HA does not begin until the surrounding environment becomes appropriate for bone mineralisation or apatite formation [9], high ion intensity should favour the apatite formation. Differences in chemical components between these two interfaces may further explain differences in mechanical properties between these two interfaces suggested in our previous study [27,28].

The influence of biomaterial dissolution rates on the microstructure of apatite deposits has been demonstrated by a number of studies [8–15,19,24]. The commonly proposed mechanism for bioactivity of calcium phosphate bioceramics involves the dissolution of calcium and phosphate ions [29]. A subsequent supersaturation of these ions in the vicinity of an implant leads to their precipitation and the formation of biological apatite [29,30]. This effect leads to the nucleation of biological apatite—both heterogeneously on the surface of the implant and also on proteins nearby [31]. Subsequently, this modified surface rapidly absorbs more protein and promotes cell adhesion [32], particularly osteoblasts, which are associated with bone bonding [33,34]. A new dissolution-precipitation mechanism was proposed in our previous study for the formation of the bone-like zone [24]. But there were discrepancies in the details of the dissolution–precipitation mechanism, mainly in the reaction sequence. Results from our present study provide evidence for the dissolution–precipitation coupling mechanism. The remarkable contrast in morphology of those two interfaces demonstrated in our study further highlights a difference in morphology of deposits apposed to implants with differing solubility.

5. Conclusion

Differences in morphology and chemical composition were demonstrated between interfaces of Sr-HA cement with cancellous bone and cortical bone. This suggests that a bioactive material's bonding to bone depends not only on the material itself, but also on the type of bone to which it bonds. Differences between these two interfaces (lower ion intensity and fine interface for cortical bone; higher ion intensity and distinct apatite layer for cancellous bone) also provide evidence for the dissolution–precipitation coupling mechanism.

Acknowledgement

We thank Dr. Lutao Weng in the Materials Characterization and Preparation Facility at The Hong Kong University of Science and Technology for assistance in ToF-SIMS experiments. The work was partially supported by the University of Hong Kong Strategic Research Area Fund on Biomedical Engineering.

Reference

[1] Hench LL, Ethridge EC. Biomaterials: an interfacial approach. In: Biophysics and Bioengineering Series, 4. New York: Academic Press; 1982. p. 62–86.
[2] Fujita Y, Yamamuro T, Nakamura T, Kotanis Ohtsuki C, Kokubo T. The bonding behavior of calcite to bone. J Biomed Mater Res 1991;25:991–1003.
[3] Dalby MJ, Di Silvio L, Harper EJ, Bonfield W. Initial interaction of osteoblasts with the surface of a hydroxyapatite-poly(methylmethacrylate) cement. Biomaterials 2001;22(13):1739–47.
[4] Fujita H, Nakamura T, Tamura J, Kobayashi M, Katsura Y, Kokubo T, et al. Bioactive bone cement: effect of the amount of glass-ceramic powder on bone-bonding strength. J Biomed Mater Res 1998;40:145–52.
[5] Senaha Y, Nakamura T, Tamura J, Kawanabe K, Iida H, et al. Intercalary replacement of canine femora using a new bioactive bone cement. J Bone Joint Surg 1996;78B:26–31.
[6] Matsuda Y, Ido K, Nakamura T, Fujita H, Yamamuro T, Oka M, et al. Prosthetic replacement of the hip in dogs using bioactive bone cement. Clin Orthop 1997;336:263–77.
[7] Fujita H, Ido K, Matsuda Y, et al. Evaluation of bioactive bone cement in canine total hip arthroplasty. J Biomed Mater Res 2000;49:273–88.
[8] Neo M, Nakamura T, Ohtsuki C, Kokubo T, Yamamuro T. Apatite formation on three kinds of bioactive material at an early stage in vivo: a comparative study by transmission electron microscopy. J Biomed Mater Res 1993;27:999–1006.
[9] Neo M, Kotani S, Fujita Y, Nakamura T, Yamamura T, Bando Y, et al. Differences in ceramics–bone interface between surface-active ceramics and resorbable ceramics: a study by scanning and transmission electron microscopy. J Biomed Mater Res 1992;26:255–67.
[10] Neo M, Kotani S, Fujita Y, Nakamura T, Yamamura T, Bando Y, et al. A comparative study of ultrastructures of the interfaces between four kinds of surface-active ceramics and bone. J Biomed Mater Res 1992;26:1419–32.
[11] Tamura J, Kitsugi T, Iida H, Fujita H, Nakamura T, Kokubo T, et al. Bone-bonding behavior of three types of bioactive bone cement containing bioactive glass or glass–ceramic powder. Bioceramics 1995;8:219–23.
[12] Okada Y, Kobayashi M, Neo M, Kokubo T, Nakamura T. Ultrastructure of the interface between bioactive composite and bone: comparison of apatite and wollastonite containing glass–ceramic filler with hydroxyapatite and β-tricalcium phosphate fillers. J Biomed Mater Res 2001;57:101–7.
[13] Fujita R, Yokoyamaa A, Nodasaka Y, Kohgo T, Kawasaki T. Ultrastructure of ceramic–bone interface using hydroxyapatite and β-tricalcium phosphate ceramics and replacement mechanism of β-tricalcium phosphate in bone. Tissue Cell 2003;35:427–40.
[14] Kotani S, Fujita Y, Kitsugi T, Nakamura T, Yamamuro T, Ohtsuki C, et al. Bone bonding mechanism of β-tricalcium phosphate. J Biomed Mater Res 1991;25:1303–15.
[15] Davies JE, Baldan N. Scanning electron microscopy of the bone–bioactive implant interface. J Biomed Mater Res 1997;36:429–40.

[16] Orly I, Gregoire M, Menanteau J, Heughebaert M, Kerebel B. Chemical changes in hydroxyapatite biomaterial under in vivo and in vitro biological conditions. Calcif Tiss Int 1989;45:20–6.
[17] Daculsi G, LeGeros RZ, Heughebaert M, Barbieux I. Formation of carbonate-apatite crystal after implantation of calcium phosphate ceramics. Calcif Tiss Int 1990;46:20–7.
[18] Porter AE, Botelho CM, Lopes MA, Santos JD, Best SM, Bonfield W. Ultrastructural comparison of dissolution and apatite precipitation on hydroxyapatite and silicon-substituted hydroxyapatite in vitro and in vivo. J Biomed Mater Res 2004;69A:670–9.
[19] Porter AE, Patel N, Skepper JN, Best SM, Bonfield W. Effect of sintered silicate-substituted hydroxyapatite on remodeling processes at the bone-implant interface. Biomaterials 2004;25:3303–14.
[20] Christoffersen J, Christoffersen MR, Kolthoff N, Barenholdt O. Effects of strontium ions on growth and dissolution of hydroxyapatite and on bone mineral detection. Bone 1997;20:47–54.
[21] Okayama S, Akao M, Nakamura S, Shin Y, Higashikata M, Aoki H. The mechanical properties and solubility of strontium-substituted hydroxyapatite. Bio-med Mater 1991;1:11–7.
[22] Li YW, Leong JCY, Lu WW, Luk KDK, Cheung KMC, Chiu KY, et al. A novel injectable bioactive bone cement for spinal surgery: a development and preclinical study. J Biomed Mater Res 2000;52:164–70.
[23] Lu WW, Cheung KMC, Li YW, Luk KDK, Holmes AD, Zhu QA, et al. Bioactive bone cement as a principal fixture for spinal burst fracture: an in vitro biomechanical and morphologic study. Spine 2001;26:2684–91.
[24] Chen QZ, Wong CT, Lu WW, Cheung KMC, Leong JCY, Luk KDK. Strengthening mechanism of bone bonding to crystalline hydroxyapatite in vivo. Biomaterials 2004;25:4243–54.
[25] Black J, Hastings G. Part I: A1, cortical bone and A2, cancellous bone. In: Handbook of biomaterial properties. New York: Chapman & Hall; 1998. p. 3–24.
[26] Lu JX, Gallur A, Flautre B, Anselme K, Descamps M, Thierry B, et al. Comparative study of tissue reactions to calcium phosphate ceramics among cancellous, cortical, and medullar bone sites in rabbits. J Biomed Mater Res 1998;42:357–67.
[27] Ni GX, Lu WW, Chiu KY, Li ZY, Fong DYT, Luk KDK. Strontium-containing hydroxyapatite (Sr-HA) bioactive cement for primary hip replacement: an in vivo study. J Biomed Mater Res 2006;77B:409–15.
[28] Ni GX, Choy YS, Lu WW, Ngan AHW, Chiu KY, et al. Nanomechanics of bone and bioactive bone cement interfaces in a load bearing model. Biomaterials 2006;27:1963–70.
[29] Sant' Anna C, Campanatic L, Gadelha C, Lourenço D, Labati-Terra L, Bittencourt-Silvestre J, et al. Improvement on the visualization of cytoskeletal structures of protozoan parasites using high-resolution field emission scanning electron microscopy (FESEM). Histochem Cell Biol 2005;12:89–97.
[30] Apkarian RP. The fine structure of fenestrated adrenocortical capillaries revealed by in-lens field-emission scanning electron microscopy and scanning transmission electron microscopy. Scanning 1997;19:361–7.
[31] Wen J, Leng Y, Chen J, Zhang C. Chemical gradient in plasma-sprayed HA coatings. Biomaterials 2000;21:1339–43.
[32] Yan L, Leng Y, Weng LT. Characterization of chemical inhomogeneity in plasma-sprayed hydroxyapatite coatings. Biomaterials 2003;24:2585–92.
[33] Lu X, Leng Y, Weng LT. TOF-SIMS study of bone mineralization on alkali-treated Ti alloy. J Material Sci 2004;39:6809–11.
[34] Weng J, Liu Q, Wolke JGC, Zhang X, de Groot K. Formation and characteristics of the apatite layer on plasma-sprayed hydroxyapatite coatings in simulated body fluid. Biomaterials 1995; 18:1027–35.